

Er³⁺ ion doped low phonon energy glass as a white light emitter

Aly Saeed^{a*}, M. A. Farag^b, W. A. Abu-raia^c

^aMathematical and Natural Science Department, Faculty of Engineering, Egyptian-Russian University, Cairo, Egypt

^bPhysics Department, Faculty of Science, Al-Azhar University, Cairo, Egypt.

^cEngineering Mathematics and Physics Department, Institute of Aviation Engineering & Technology, Giza, Egypt

White light emitters remain in the need of continual development and research for new materials. In this context, a low phonon energy glass containing Er³⁺ ions was prepared using the conventional melt/casting technique. The chemical compositions of the synthesized materials were analyzed using X-Ray Fluorescence (XRF) measurements. X-Ray Diffraction (XRD) pattern strongly affirms the non-crystalline essence of the produced materials. The behavior of both density and Fourier Transform Infrared (FTIR) spectroscopy denoted that the Er³⁺ ions have a modifier role and non-bridging oxygens NBOs were formed inside the studied glass network. The studied glasses have low phonon energy, ranging from 647 to 659 cm⁻¹. The obtained results of the thermal, thermo-mechanical, mechanical, and optical properties were discussed in light of the structural changes brought about by inserting Er³⁺ ions inside the studied network. The present glasses have high thermal stability, high thermal expansion, and high refractive index. With the increase of Er³⁺ ion content, the Vickers microhardness VMH decreased from 3.78 GPa to 3.20 GPa. Under near ultraviolet NUV 380 nm excitation wavelength, three emission bands; blue, green, and red are observed. The white light is possible by a suitable combination of these colors. The cool white light emission was confirmed using CIE 1931 chromaticity diagram and correlated color temperature values. According to the obtained results, the studied glasses are nominated as a white light emitter in photonic applications.

Keywords: White light materials, Luminescent materials, Heavy metals oxyfluorophosphates glass, Er³⁺ ion

Paper information:

Receive Date: 10 August 2021; Revise Date: 26 August 2021; Accept Date: 01 September 2021
;Publish Date: 04 September 2021

*Corresponding Author: aly-saeed@eru.edu.eg

1. Introduction

Photonic devices for creating, manipulating, or detecting light occupy a supreme rank in modern technology. Luminescent materials have numerous applications in many optical and optoelectronic devices. Luminescent materials must be easily excited by light of the appropriate wavelength and must have a high quantum efficiency. In the manufacturing and development of luminescent materials, the utilization of suitable host and dopant ions is fateful [1-6].

Trivalent lanthanum ions, Ln^{3+} extensively investigated as emitter ions due to the harmony of their fine emission spectra with large numbers of photonic devices. Several f-f Ln^{3+} ions transitions generate white light luminescence, which is consisting of red, orange, yellow, green, cyan, blue, and violet [7-9]. Host materials that have low phonon strength are a superior candidate to reduce nonradiative NR loss by multiphonon relaxation MPR and hence generate high quantum yield. The oxide glass, such as phosphate, borate, and silicate has a significant role as host photonic materials [10-11]. Among them, the phosphate network is considered an efficient optical host due to its high thermal stability, high transparency over the UV – visible wavelength range, and especially good solubility of rare-earth ions. The lack of chemical durability of the phosphate glass network is usually treated via inlaying the phosphate network with suitable alkali and alkaline earth oxides [12-14]. Fluoride host materials have a high quantum yield due to their ionic bonds and low phonon energy [14-15]. Heavy metal ions have a combination of desirable optical, mechanical, and thermal properties. Heavy metals oxide glasses have an interesting role in photonic devices because of their optical properties, such as high refractivity and optical nonlinearity [16-19]. Hence, heavy metals oxyfluorophosphate glasses are promising hosts for several photonic applications because they have both oxides and fluorides characteristics. At the low ratios of phosphate/fluoride, fluoride ligation dominates on the local environment of the Re^{3+} ions, which is significant for high quantum yield and phonon-assisted energy transfer processes [13-15]. Trivalent erbium ion Er^{3+} is usually used in various hosts as a dopant because of its peculiar optical properties. Generally, Er^{3+} ion is an ideal candidate for photonic applications due to its rich energy levels in the ultraviolet, visible, and near-infrared ranges [16-19]. Since white light emitters are still in continuous need of development, numerous studies in this regard using different host materials and doping were carried out. In 2014, E. H. Song et al. were succeeded in generating white light from Yb^{3+} - Tm^{3+} - Mn^{2+} tri-doped perovskite nanocrystals using a 976 nm [7]. Norfatirah Muhamad Sarih et al. in 2019 measured the white light that emitted from three compounds, furocoumarin, dansyl aniline, and 7-hydroxycoumarin-3-carboxylic acid when excited by wavelengths ranged from 340 nm to 370 nm [33].

Because of the foregoing, the white light emission from a developed P_2O_5 -ZnO-PbO- Bi_2O_3 -NaF-LiF glass system inlaid by Er^{3+} ions was examined. The emission spectra were generated using NUV 380 nm excitation wavelength. XRF, XRD, density, FTIR, Differential Scanning Calorimetry DSC thermograms, thermal expansion coefficient, Vickers microhardness VMH, and optical absorption were measured and discussed in detail to explore the impact of Er^{3+} ions on the prepared host glass.

2. Materials and Experimental Techniques

Appropriate amounts of high purity oxides and fluorides imported from Sigma Aldrich company were synthesized, mixed, and melted to prepare heavy metals oxyfluorophosphate glass containing Er^{3+} ions. The chemical formula of studied glasses are $45P_2O_5-(20-x)ZnO-20PbO-5Bi_2O_3-5NaF-5LiF-xEr_2O_3$, where x was varied as 0, 0.5 and 1 mol%. The raw materials of the suggested glass system were mixed thoroughly in a mortar and fused in an alumina crucible at 1100 °C for two hours. During melting, the melt was shaken periodically to get high homogenous free bubble liquid. Then, the obtained melt was quenched on a 350 °C preheated stainless steel mold and annealed below the glass transition temperature for 2 h to eliminate the internal thermal stresses. The obtained materials were divided into two parts, one of them was ground and the other was polished to get a smooth surface. The powder form was used in XRF, XRD, FTIR, DSC, measurements. On the other hand, the bulk form was used in density, Vickers microhardness, thermal expansion, optical absorption, and emission measurements.

To get the accurate chemical compositions of the studied glasses after a probable loss of some constituents during the preparation and also to estimate the impurity in the used raw materials, X-ray fluorescence was measured by PHILIPS X' Unique –II spectrometer with automatically specimen changer. The structural phase of the produced materials was examined by X-ray diffraction mechanism, Shimadzu XD3A radiation with $CuK_{\alpha} = 1.54056 \text{ \AA}$. Bulk density was measured using the Archimedes method by measuring the glass piece weight in air and its weight in xylene liquid [20-21]. The value of the density was averaged over five such measurements. Infrared absorption spectra were measured by FTIR spectrophotometer JASCO FT – IR – 300 using the reference material KBr in the spectral range 400 – 4000 cm^{-1} . Differential Scanning Calorimetry DSC thermograms measurements were performed by TA Instruments SDT Q600 in an open platinum pan at a heating rate of 10 °C/min up to 600 °C in a high purity nitrogen atmosphere at flow rate of 15 Psi. The glass transition T_g and onset of crystallization T_c temperatures were identified. The $1.5 \times 1.5 \times 0.2 \text{ cm}^3$ samples were used to measure the thermal expansion via a computerized dilatometer type (NETSCH, 402 pc, Germany) at heating rate of 10 °C/min from room temperature to the dilatometric softening

temperature. Thermal expansion coefficient α , glass transition temperature T_g , and softening temperature T_s were obtained. The

Vickers microhardness was measured using HMV Shimadzu Micro Hardness Tester with a load of 490.3 mN by a force duration of 10 seconds. Five randomly reading was measured on the same smooth surface for each sample. A 0.2 cm glass thickness was polished for UV-visible absorption spectra measurements in the spectral range 190–1100 nm using Jenway 6405 UV/Vis Spectrophotometer. The emission spectra were measured on a flat and smooth specimen using a SPEX spectrofluorimeter (Model Fluorolog-II, SPEX CertiPrep, Metuchen, NJ) in the wavelength region of 300–900 nm under 380 nm excitation wavelengths emitted from 150W Xenon lamp.

3. Results and Discussion

The obtained chemical compositions from the XRF analysis are listed in **Table 1**. Little amounts of impurities, Ca, K, Fe, Ni, Sr, Zr, Cd, and Ru ranged from 0.32 to 0.79 mol% are found in the produced glasses.

Table 1: Chemical compositions of the prepared glasses using XRF

Er ³⁺ Concentration mol%	P ₂ O ₅	ZnO	PbO	Bi ₂ O ₃	NaF	LiF	Er ₂ O ₃
0	44.594	19.995	20.003	5.05	4.971	5.021	0
0.5	44.906	19.305	19.803	5.275	4.981	4.889	0.521
1	44.942	18.926	19.73	5.045	5.011	4.962	1.094

A broad and weak intense hump is observed in the X-ray diffraction patterns for the obtained materials as shown in **Figure 1**. The observed pattern indicates that the prepared materials are fully amorphous.

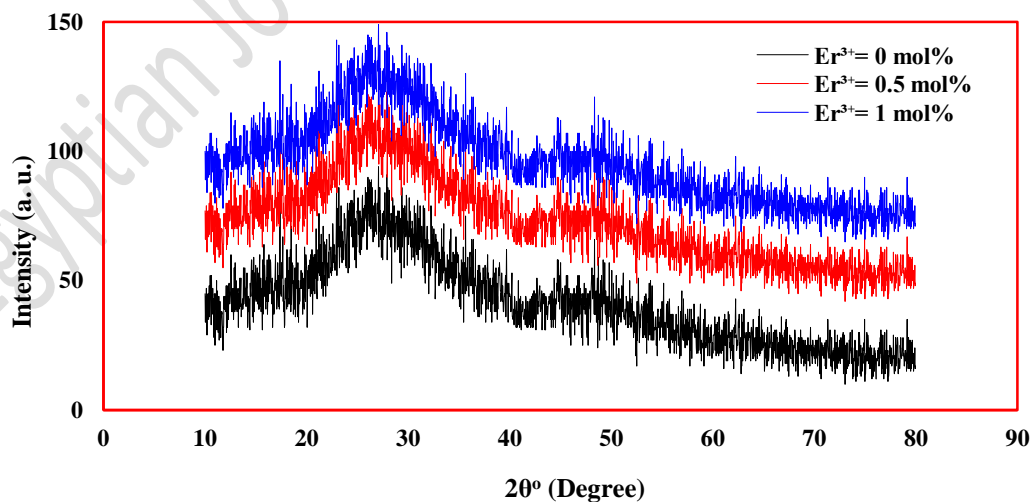


Fig 1: Diffraction pattern of the studied materials

The compositional dependence of density ρ and molar volume V_m are tabulated in **Table 2**. The value of molar volume V_m was evaluated using the molecular weight of the glass constituents M and the experimental density ρ according to the formula [20-21].

$$V_m = \frac{M}{\rho} \quad (1)$$

Density diminution and molar volume augmentation were attributed to the phosphate chains depolymerization, which occurred because of enriching the studied network by Er^{3+} ions. The inlaying of the studied host by Er^{3+} ions breaks the P-O-P chain and forms non-bridging oxygens causing augmentation of space between the phosphor atoms. The average phosphor-phosphor separation d_{p-p} , which was calculated according to the relation 2 [20-21] and listed in **Table 2** confirmed the spacing of the phosphor atoms.

$$d_{p-p} = \left(\frac{V_M^P}{N_A} \right)^{\frac{1}{3}} \quad (2)$$

$$V_M^P = \frac{V_M}{2(1 - X_p)}$$

where the V_M^P is the volume that contains one mole of phosphor within the obtained network and X_p molar fraction of P_2O_5 .

These results refer to that the erbium ions occupy the interstices spaces in the present glass network. Hence, the Er^{3+} ions enter as a modifier in the studied glass network. The Er^{3+} ions insertion leads to the expansion of the studied glass network.

Table 2: Density ρ , molar volume V_m , average phosphor - phosphor d_{p-p} , glass transition temperature T_g , crystallization temperature T_c , thermal stability ΔS , softening temperature T_s , thermal expansion coefficient α Vickers microhardness VMH, optical band gap E_g Urbach energy E_u , refractive index n of the studied glasses

Er^{3+} ions (mol%)	0	0.5	1
ρ (gm/cm ³)	5.557	5.279	5.106
V_m (cm ³ /mol)	32.951	34.407	35.532
d_{p-p} (°A)	3.678	3.731	3.772
DSC T_g (°C)	365	361	357
From thermal expansion	368	359	362
T_c (°C)	476	481	485
ΔS (°C)	111	120	128
T_s (°C)	311	306	302
$\alpha \times 10^{-7}$ (°C ⁻¹)	148	153	157
VMH (GPa)	3.78	3.48	3.20
E_g (eV)	3.45	3.35	3.30
E_u (eV)	0.312	0.345	0.401
n	2.285	2.308	2.320

The functional groups in the studied glasses were determined through FTIR absorption spectra. In **Figure 2**, four clear bands are observed in the free Er^{3+} ions sample. Two intense bands at 647 and 1492 cm^{-1} and weak bands at 765 and 947 cm^{-1} are determined. According to the obtained FTIR spectra, the symmetric stretching modes $(\text{P-O-P})_s$ linkages of Q^1 units are present at the wavenumber 647 cm^{-1} , while the asymmetric stretching modes $(\text{P-O-P})_{as}$ linkages are located at 765 cm^{-1} . The band at 947 cm^{-1} is related to asymmetric stretching vibrations of PO_4^{3-} tetrahedra (P-O- ionic group). The fixed band at 1492 cm^{-1} is assigned to the asymmetric stretching of double bonded P=O modes [12, 14, 22]. No additional bands are observed in the Er^{3+} ions doped samples. With the accretion of Er^{3+} ions concentration, the peaks have been shifted to longer wavenumber and their amplitudes have been increased. These observations are in harmony with the obtained results of density, which confirm the formation of non-bridging oxygens inside the studied network and the modifier role of Er^{3+} ions. The phonon energy is a crucial factor in the choice of the host luminescent materials as mentioned in the introduction. Also, it is known that the phonon energy is always compatible with the highest IR band. The maximum phonon energy for the studied glasses has ranged from $647\text{-}657\text{ cm}^{-1}$, which is considered the lowest range compared to the other host glasses like silicate (1100 cm^{-1}), germanate (845 cm^{-1}), and tellurite (790 cm^{-1}) glasses [6, 12, 23-25].

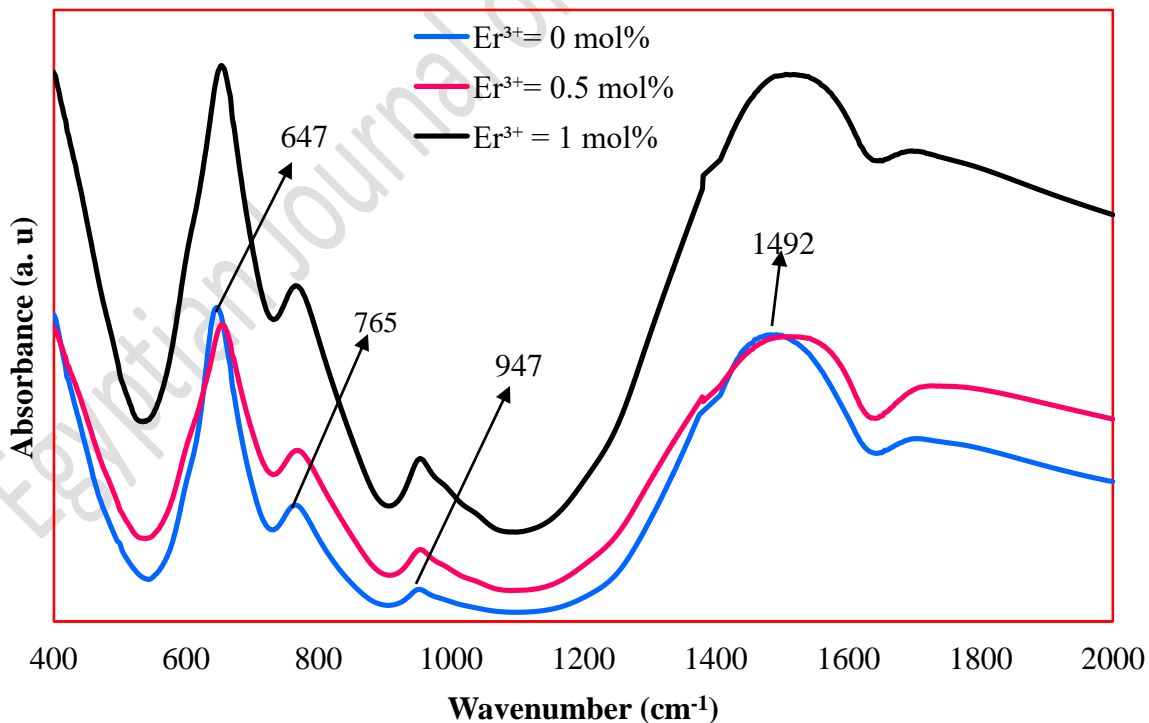


Fig 2: FTIR spectra of the studied glasses

Based on the discussion of density and FTIR results, the Er^{3+} ions incorporated into the present glass network as modifiers have lead to breaking down the oxygen bridge atoms causing loss of the packing of the glass network. As a result, a decrease in T_g is observed as listed in **Table 2**. The diminution of T_g with the increase of Er^{3+} ions concentration implies that the Er^{3+} ions enrich the glass forming ability. The obtained values of T_g from DSC agree with those obtained from the thermal expansion coefficient measurements with a little variation ranging from 2 to 5 °C as listed in **Table 2**. The decrease in T_g is evidence of the rigidity weakness of the glassy framework. The decrease of T_g and increase of T_c enhance the thermal stability ΔS of the present glasses. The obtained values of the thermal stability, which have been evaluated by the temperature gap between T_c and T_g [14] are listed in **Table 2**. The thermal stability of the glass is a considerable factor in photonic devices, in which high thermal stability values are always desirable. The addition of the Er^{3+} ions has improved the thermal stability of the prepared glass samples. The value of $\Delta S > 100$ °C indicates that the present glass samples exhibit superior thermal stability and could be useful for photonic applications.

The insertion of the Er^{3+} ions to the present glass samples has also increased the thermal expansion coefficient as listed in **Table 2**. This behavior shows the reduction in the glass network connectivity due to the formation of non-bridging oxygen atoms. The addition of the Er^{3+} ions has macerated the chains of phosphate through damage the P-O-P chain and has formed ionic cross-linking bonding between the broken bonds and thus, creating non-bridging oxygens. Also, this rigidity reduction has led to an obvious and remarkable change in the softening temperature T_s as listed in **Table 2**. The T_s values have changed from 311°C for the free Er^{3+} glass to 302°C for the glass contains 1mol% of Er^{3+} .

As clearly seen from **Table 2**, the microhardness is decreased with the increment of Er^{3+} ions concentration. This is due to the diminution in packing density. It means that there is a breaking of some P–O–P bonds per volume in the glass network, which decreases the resistance of deformation. In other words, the decrease in microhardness is consistent with the weakening of the glass network.

The optical absorption spectra of the Er^{3+} ions free and doped glasses are displayed in **Figure 3**. No absorption bands are observed in the free sample. So, the observed large numbers of the absorption bands in the doped samples are due to the transitions through Er^{3+} ions energy levels. The absorption bands in the spectra arise from intra-configuration $f - f$ transition from the ground state $^4I_{15/2}$ of Er^{3+} ion to the different excited states. In the sample of 0.5 mol% of Er^{3+}

ions, the observed peaks centered at 361, 376, 406, 447, 484, 518, 543, 651, and 978 nm are assigned to the transition from the ground state $^4I_{15/2}$ to $^4G_{9/2}$, $^4G_{11/2}$, $^4F_{3/2}$, $^4F_{5/2}$, $^4F_{7/2}$, $^2H_{11/2}$, $^4S_{3/2}$, $^4F_{9/2}$, and $^4I_{11/2}$, respectively [20-21]. Besides these bands, an additional band was observed at 1 mol % of Er^{3+} ions concentration and centered around 800 nm, which is attributed to the transition to $^4I_{9/2}$ [21-21].

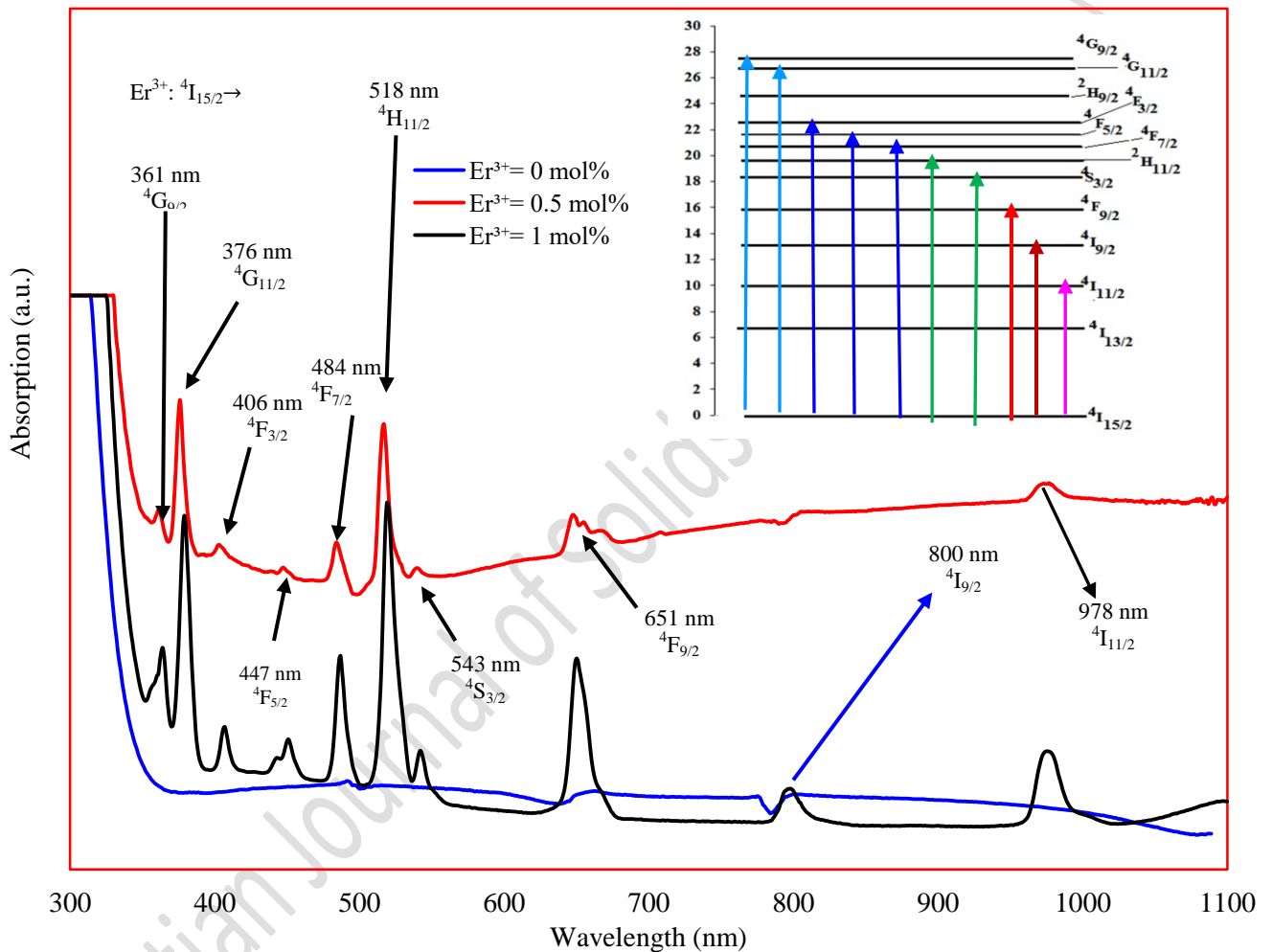


Fig 3: The optical absorption spectra of the studied glasses

For semiconducting materials, phonon absorption or emission is stimulated during the photon absorption mechanism. The absorption of photon energy takes place through the phonon absorption when $E_g - E_{ph}$, where E_g is the indirect band gap and E_{ph} represents the phonon absorption. On the other hand, the photon is absorbed during phonon emission when the photon energy is $E_g + E_{ph}$. The value of the optical band gap E_g for the indirect allowed transition is deduced through solving $E_g - E_{ph}$ and $E_g + E_{ph}$ [26-27]. **Figure 4** shows the relation between

$(\alpha h\nu)^{1/2}$ and the photon energy $h\nu$ for Er^{3+} ions free sample as a representative figure. The Urbach energy E_u has been calculated relying on the Urbach - Tauc's model [23]

$$\alpha(\nu) = \beta \exp\left(\frac{h\nu}{E_u}\right) \quad (3) \quad \text{where, } \beta \text{ is a constant.}$$

The Urbach energy is deduced through plotting $\ln \alpha$ against $h\nu$ and by taking the slope of the straight-line tangents of the plotted curve.

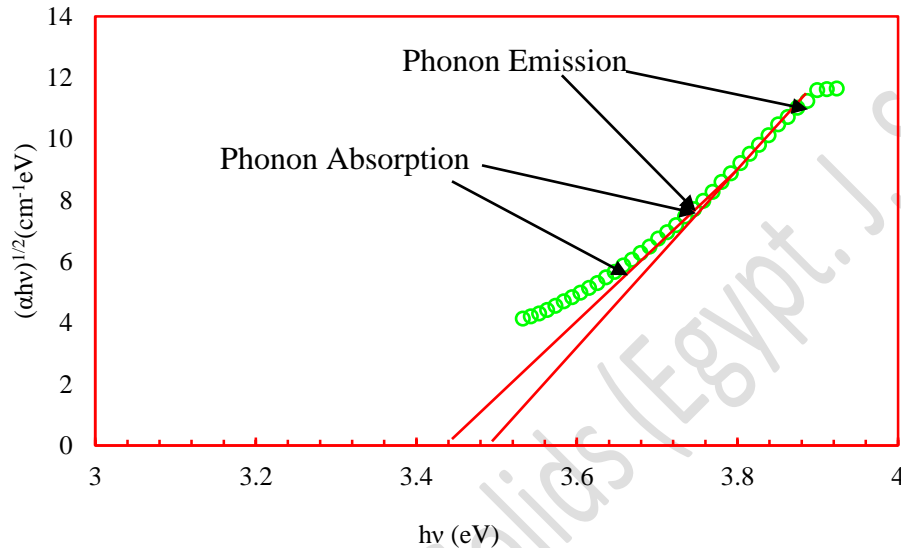


Fig 4: $(\alpha h\nu)^{1/2}$ versus photon energy for the indirect allowed transition of the obtained glasses

The obtained results of the optical band gap and Urbach energy are recorded in **Table 2**. The reduction of the optical band gap is attributed to the decrease in donor centers. The augmentation of E_u indicates the increase of the disorder in the studied glass network. The disorder in the studied glass network arises due to the formation of the imperfections as anomalous bonds such as the deformation in bond angle, dangling bonds, and/or NBOs in the glass samples.

The values of refractive indices n , which have been calculated from equation 4 [28-29] are listed in **Table 2**. The higher value of the refractive indices are attributed to the formation of non-bridging oxygens in the glass network. The non-bridging oxygen atoms are much more polarizable than bridging oxygen. The glass samples with a more fragmented network exhibit higher refractive indices.

$$\frac{n^2 - 1}{n^2 + 2} = 1 - \sqrt{\frac{E_g}{20}} \quad (4)$$

Figure 5a displays the emission spectra of the studied glass samples after pumping by NUV 380 nm. In 0.5 and 1 mol% of Er^{3+} doped glass, three emission bands are observed in the

blue, green, and red regions of the spectra and located at 453, 552, and 626 nm respectively. The blue peak at 453 nm matches the transition ${}^4F_{5/2} \rightarrow {}^4I_{15/2}$. The observed intense green peak at 552 nm originates from the transition ${}^4S_{3/2} \rightarrow {}^4I_{15/2}$. The highest intensity of this band is due to the change in the coordination number of Er^{3+} ions in the present glass. The red peak at 626 nm is due to ${}^4F_{9/2} \rightarrow {}^4I_{15/2}$ transition [30-35]. To get more understanding of the energy transfer mechanisms between different energy levels of Er^{3+} ion, the energy schematic diagram is illustrated in **Figure 5b**. First, the ground state electrons ${}^4I_{15/2}$ of Er^{3+} ion are excited to the ${}^4G_{11/2}$ using 380 nm excitation wavelength. The Er^{3+} ion populated at ${}^4G_{11/2}$ level relaxes rapidly and non-radiatively NR to the long-lived ${}^4F_{5/2}$, ${}^4S_{3/2}$, and ${}^4F_{9/2}$ levels through the multi-phonon relaxation process MRP [30-35]. The electrons at the ${}^4F_{5/2}$ level probably also decay to the ${}^4S_{3/2}$ state through the MRP. The electrons at ${}^4S_{3/2}$ can also decay non-radiatively to populate long living ${}^4F_{9/2}$ level [30-35]. The electrons at ${}^4F_{5/2}$ decay rapidly through radiative relaxation to the ground state ${}^4I_{15/2}$ level producing blue emission at 453 nm [30-35]. The strong green emission peak at 552 nm is arisen by radiative relaxation from the ${}^4S_{3/2}$ level to the ground state ${}^4I_{15/2}$ level [30-35]. The red emission peak at 626 nm is originated through rapid decay from ${}^4F_{9/2}$ level to the ground state ${}^4I_{15/2}$ [30-35]. The white light emission could be produced through a proper combination of the obtained three emission bands: blue, green, and red. The white light can be controlled by tuning the green/red/blue ratio. The CIE-1931 chromaticity coordinates for $Er^{3+} = 0.5$ and 1 mol% are (0.321, 0.377) and (0.322, 0.384), respectively as shown in **Figure 6**. These chromaticity coordinates are highly close to those of the standard white light (0.33, 0.33). McCamy's approximate formula $CCT = -449n^3 + 3525n^2 - 6823.3n + 5520.33$ has been used to estimate the correlated color temperature (CCT) in Kelvin based on the CIE chromaticity coordinates [35]. The CCT value for 0.5 mol% of Er^{3+} is 5925 K and 5874 for 1 mol% of Er^{3+} , which means that the produced glass samples located in the zone of cool white light. The occurrence of the studied glass in the cool white light area indicates the feasibility of employing it as white light emitting diodes w-LEDs.

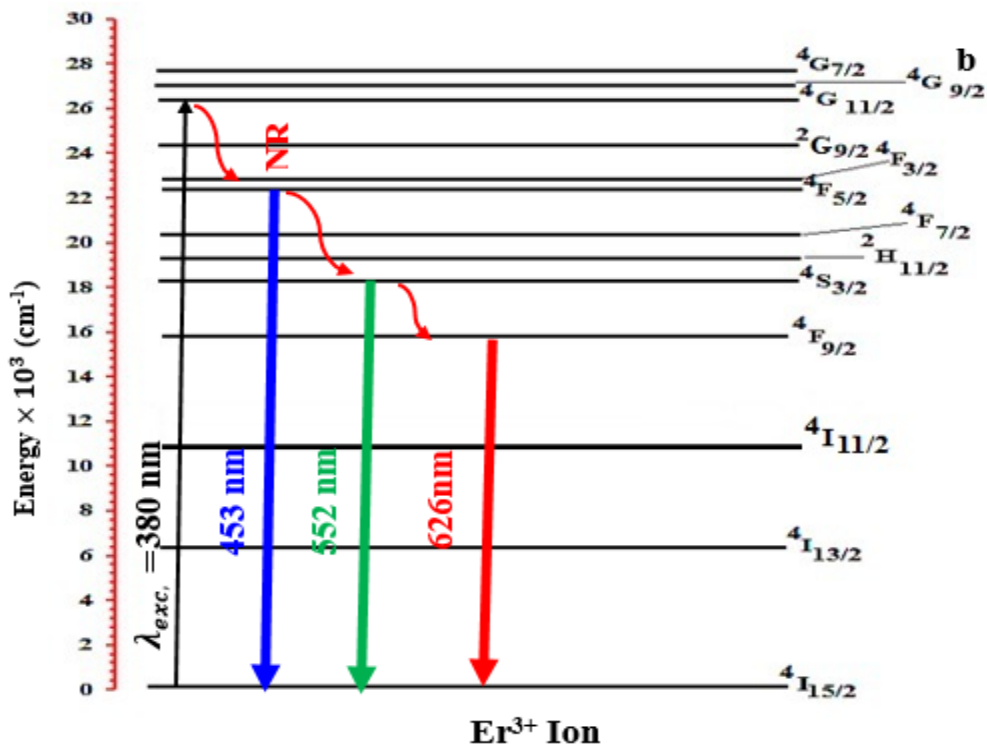
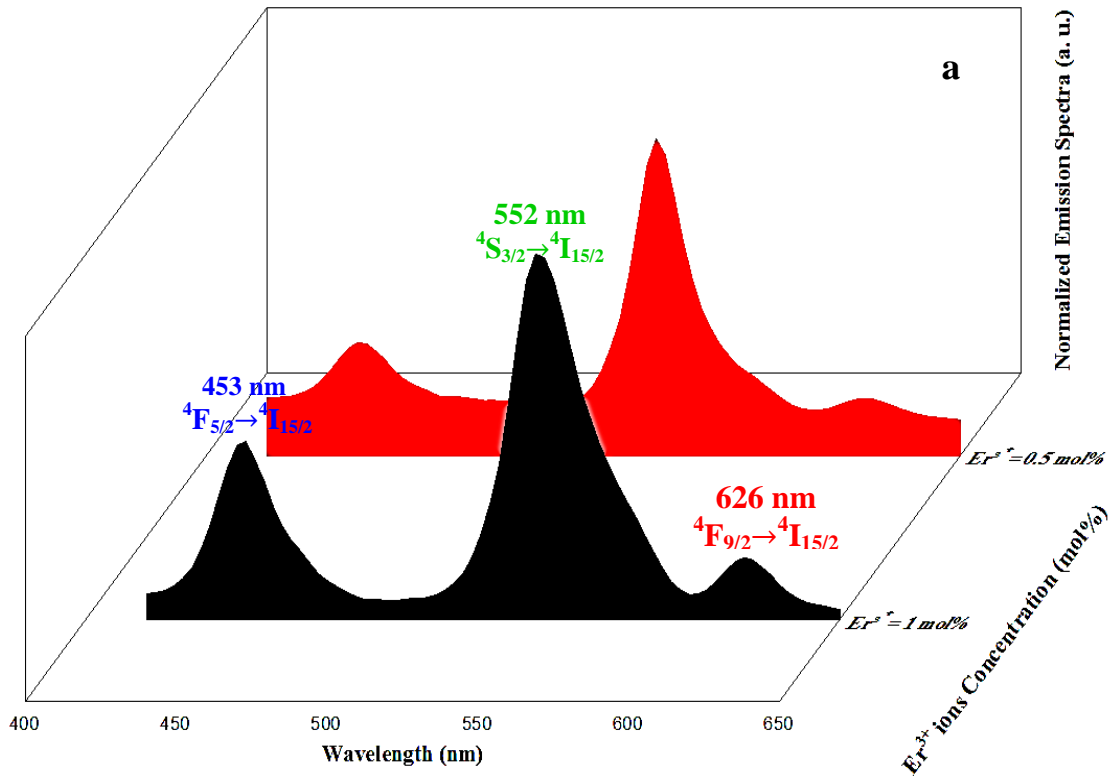


Fig 5: a) The emission spectra b) the possible transition in Er^{3+} ion energy levels for the produced glass samples under 380 nm excitation wavelength

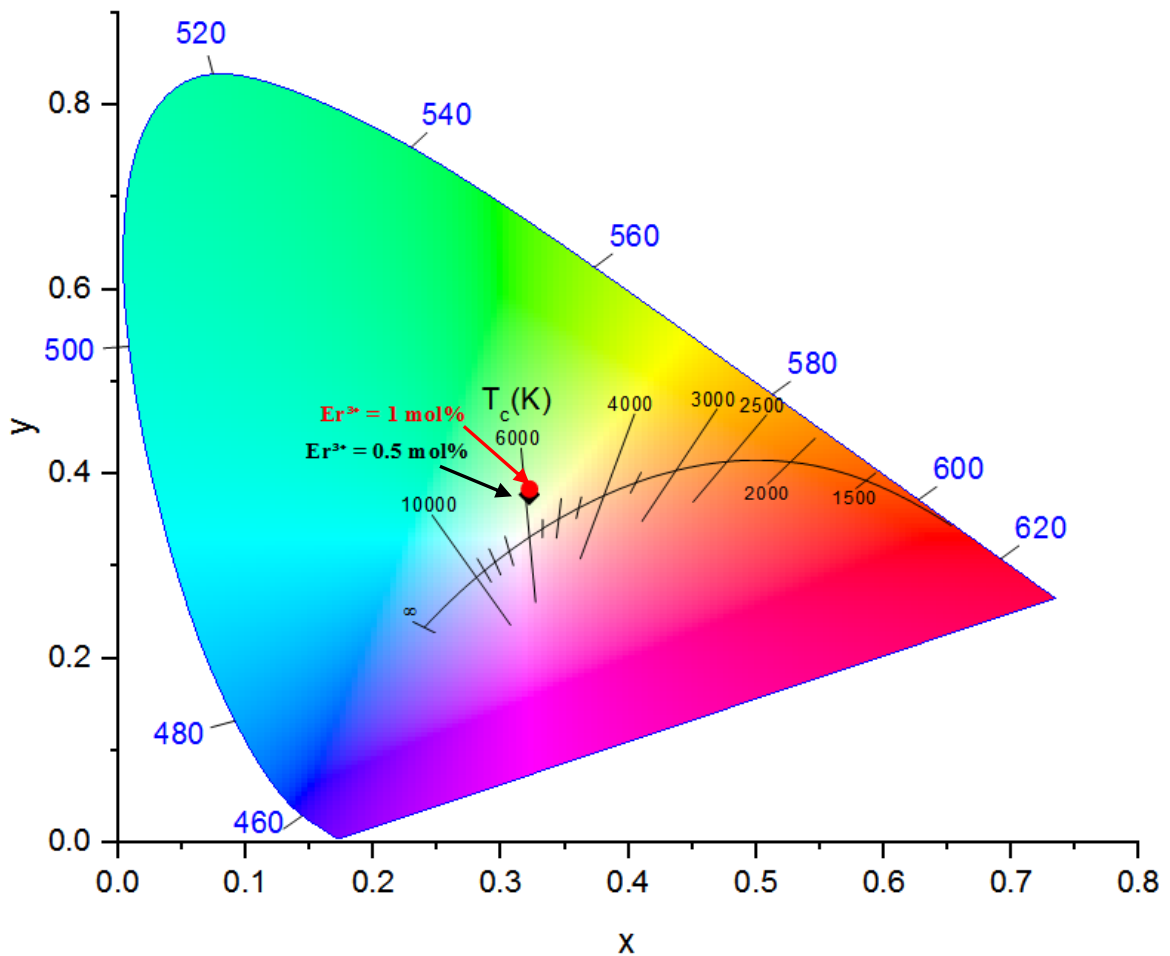
CIE 1931

Figure 6: CIE-1931 chromaticity chart of the studied glass samples

4. Conclusion

Emitted white light from Er^{3+} ions activated in developed heavy metals oxyfluorophosphate glass has been studied. The density and FTIR results showed that the Er^{3+} ions act as a modifier in the produced host glass. The formed non-bridging oxygens in the studied glass network have caused a loss in the glass network connectivity. The weakness in the studied glass rigidity has appeared in the dwindling of microhardness and glass transition temperature. The studied glass samples have high thermal stability, high thermal expansion, and low phonon energy ($647\text{-}659\text{ cm}^{-1}$) that are considered the most important requirements of photonic materials. Harmonic behavior between the density, FTIR, thermal, thermo-mechanical, and mechanical results are observed. Three colors: blue, green, and red have been generated when the studied glass samples have been pumped by the NUV wavelength 380 nm. Accordingly, the white light based on a suitable combination of the obtained colors can be tuned

in the studied glass samples. The emission of white light is proved through the CIE chromaticity diagram. The correlated color temperature values match the standard cool white region. The superior characteristics of the developed Er^{3+} doped heavy metals oxyfluorophosphate glass samples can be attractive for various photonic devices operating in the visible region, especially as solid-state white light emitters.

References

- 1.P. P. Zak, V. A. Lapina, T. A. Pavich, A. V. Trofimov, N. N. Trofimova, and Y. B. Tsaplev, *Russian Chemical Reviews*, 86(9) (2017) 831 – 844.
- 2.C. Shi, Y. Zhu, G. Zhu, X. Shen, and M. Ge, *Journal of Materials Chemistry C*, 6 (2018) 9552-9560.
- 3.D. Li, J. Wang, and X. Ma, *Advanced Engineering Materials*, 6, 1-27 (2018).
- 4.K. Annapoorani, K. Maheshvaran, S. Arunkumar, N. Suriya Murthy, and K. Marimuthu, *Luminescent Materials*, 135(25) (2015) 1090-1098.
- 5.Y. Li, Y. Fang, N. Hirosaki, R.-J. Xie, L. Liu, T. Takeda, and X. Li, *Materials*, 3 (2013) 1692-1708.
- 6.Ch. Basavapoornima, C. R. Kesavulu, T. Maheswari, W. Pecharapa, S. R. Depuru, and C. K. Jayasankar, *Journal of Luminescence*, 227 (2020) 117585.
- 7.Q. Ren, Y. Zhao, X.Wu, and O. Hai, *Optics & Laser Technology*, 136, (2021) 106774.
- 8.Y. Zhang, H. Lei, G. Li, L. Zeng, and J. Tang, *Optical Materials*, 99, (2020) 11-20.
- 9.S. Jiang, P. Zeng, L. ing Liao, S. eng Tian, H. Guo, Y. Chen, C. Duan, and M. Yin, *Journal of Alloys and Compounds*, 617 (2014) 538–541.
- 10.G. Galleani, C. Doerenkamp, S. Santagneli, C. J. Magon, A. S. S. de Camargo, and H. Eckert, *The Journal of Physical Chemistry C*, 123(51) (2019) 31219–31231.
- 11.M. A. Marzouk, S. M. Abo-Naf, H. A. Zayed, and N. S. Hassan, *Journal of Applied Spectroscopy*, 84(1), (2017) 162-169.
- 12.M. Kuwik, J. Pisarska, and W. A. Pisarski, *Materials*, 13 (2020) 1-20.
- 13.G. Galleani, S. H. Santagneli, Y. k. Ledem, Y. Messaddeq, O. Janka, R. Pöttgen, and H. Eckert, *The Journal of Physical Chemistry C*, 122(4) (2018) 2275–2284.
- 14.M. Lesniak, J. Zmojda, M. Kochanowicz, P. Miluski, A. Baranowska, G. Mach, M. Kuwik, J. Pisarska, W. A. Pisarski, and D. Dorosz, *Materials*, 12 (2019) 1-31.
- 15.M. Naftaly and A. Jha, *Journal of Applied Physics*, 87 (2000) 2098-2104.
- 16.A. Saeed, Y. H. Elbashar, and S. U. El Kameesy, *Silicon*, 10 (2018) 185-189.
- 17.M. Bosca, L. Pop, G. Borodi, P. Pascuta, and E. Culea, *Journal of Alloys and Compounds*, 479 (2009) 579–582.

- 18.N. Chanthima, N. Kiwsakunkran, J. Kaewkhao, and N. Sangwaranatee, *Journal of Metals, Materials and Minerals*, 29(2) (2019) 58-63.
- 19.H. Sun, S. Xu, Shixun Dai, L. Wen, J. Zhang, L. Hu, and Z. Jiang, *Journal of Non-Crystalline Solids*, 351 (2005) 288–292.
- 20.A. Saeed, Y. H. Elbashar, and S. U. El Khameesy, *Silicon*, 10 (2018) 569–574.
- 21.A. M. El-Batala, A. Saeed, N. Hendawy, M. M. El-Ok, and M. K. El-Mansy, *Journal of Non-Crystalline Solids*, 559 (2021) 120678.
- 22.A. A. El-Kheshen, F. H. El-Batal, and S. Y. Marzouk, *Indian Journal of Pure & Applied Physics*, 46 (2008) 225-238.
- 23.S. Jana, B. Karmakar, and P. Kundu, *Materials Science-Poland*, 25(4) (2007) 1127-1134.
- 24.D. Möncke and H. Eckert, *Journal of Non-Crystalline Solids: X*, 3 (2019) 1-15.
- 25.K. Yoshimoto, A. Masuno, M. Ueda, H. Inoue, H. Yamamoto, and T. Kawashima, *Scientific Reports*, 7(1) (2017) 1-9.
- 26.H. Y. Morshidy and M. S. Sadeq, *Journal of Non-Crystalline Solids*, 525 (2019) 1-6.
- 27.M. S. Sadeqa and H. Y. Morshidy, *Ceramics International*, 45 (2019) 18327–18332.
- 28.A. Saeed, Y. H. Elbashar, and R. M. El shazly, *Optical and Quantum Electron*, 48(1) (2016) 1-10.
- 29.S. L. Srinivasa Rao, G. Ramadevudu, Md. Shareefuddin, A. Hameed, M. Narasimha Chary, and M. Lakshmiopathi Rao, *International Journal of Engineering, Science and Technology*, 4(4) (2012) 25-35.
- 30.D. Pugliese, N. G. Boetti, J. Lousteau, E. Ceci-Ginistrelli, E. Bertone, F. Geobaldo, and D. Milanese, *Journal of Alloys and Compounds*, 657 (2016) 678-683.
- 31.C. R. Kesavulu, H. J. Kim, S. W. Lee, J. Kaewkhao, N. Wantana, S. Kothan, and S. Kaewjaeng, *Journal of Alloys and Compounds*, 683 (2016) 590-598.
- 32.F. Zhang, Z. Xiao, L. Yan, F. Zhu, and A. Huang, *Applied Physics A*, 101 (2010) 777–780.
- 33.N. M. Sarih, P. Myers, A. Slater, B. Slater, Z. Abdullah, H. A.tajuddin, and S. Maher, *Scientific Reports*, 9 (2019) 1-8.
- 34.W. Strek, B. Cichy, L. Radosinski, P. Gluchowski, L. Marciniak, M. Lukaszewicz, and D. Hreniak, *Light: Science & Applications*, 4 (2015) 1-8.
- 35.L. Vijayalakshmi, K. Naveen Kumar, K. Srinivasa Rao, and P. Hwang, *Journal of Molecular Structure* 1155 (2018) 394-402.